



43rd European Rotorcraft Forum  
Milan, Italy, 12-15th September,  
2017  
Paper 522

## Whirl and Stall Flutter Simulation Using CFD

**Ross J. Higgins**

r.higgins.1@research.gla.ac.uk  
CFD Laboratory, School of Engineering  
James Watt South Building  
University of Glasgow, G12 8QQ, U.K.

**George N. Barakos**

George.Barakos@glasgow.ac.uk  
CFD Laboratory, School of Engineering  
James Watt South Building  
University of Glasgow, G12 8QQ, U.K.

This paper presents recent research on numerical methods for whirl and stall flutter using computational fluid dynamics. The method involves coupling of the HMB3 CFD solver of the University of Glasgow and a NASTRAN derived structural model. Based upon a literature survey, a significant amount of research has been conducted on the numerical investigation of tiltrotors, with a focus on the XV-15 and V-22 aircraft. Within this paper, the coupling procedure is presented along with a steady CFD computation to highlight the accuracy of the high-fidelity method. In addition to this, a simple method is used to investigate the whirl flutter boundary of a standard propeller and the XV-15 blade.

### 1 INTRODUCTION

Whirl and stall flutter are potentially dangerous phenomena for turboprop aircraft, tiltrotors and helicopters. As a result, the present work is looking at methods to determine the onset of flutter and mitigate its effects.

Whirl flutter is defined as the coupling between the gyroscopic and aerodynamic modes within an idealised propeller-nacelle system [1]. Such a conclusion was derived following the expensive work carried out by NASA in the 1960's following the loss of two Lockheed Electra aircraft to whirl flutter. The work carried out involved numerical and experimental investigations. The numerical technique involved the use of rigid beam model with a spring-damper system. This was investigated with aerodynamics derived via a derivative based approach [2] and an eigenvalue analysis conducted

to determine the stability boundary [3]. A comparison between these numerical methods and the experimental work was conducted with a conservative boundary obtained using the numerical techniques. To gain closer quantitative results, modifications to the experimental models [4, 5] were made until a propeller-nacelle like structure was derived [6].

With the return to service of the Lockheed Electra aircraft, interest in whirl flutter was lost until the development of tiltrotors. A tiltrotor aircraft combines the vertical take off capability of a helicopter with the forward flight efficiency and speed of a turboprop aircraft, however due to the configuration of such a vehicle, one of the limiting factors within the forward flight capabilities is due to whirl flutter. As a result, the full understanding of the stability boundary is required.

---

Copyright Statement© The authors confirm that they, and/or their company or organisation, hold copyright on all of the original material included in this paper. The authors also confirm that they have obtained permission, from the copyright holder of any third party material included in this paper, to publish it as part of their paper. The authors confirm that they give permission, or have obtained permission from the copyright holder of this paper, for the publication and distribution of this paper as part of the ERF2017 proceedings or as individual offprints from the proceedings and for inclusion in a freely accessible web-based repository.

With further development of technology, more comprehensive studies were conducted for tiltrotor aircraft, with NASA being at the forefront. The development of numerical tools such as CAMRAD [7], which is a blade element model with dynamic stall capabilities [8], allowed for a whirl flutter investigation to be conducted on the XV-15 and V-22 aircraft [9, 10, 11, 12, 13]. In addition to this, the development of the NASA Langley Transonic Dynamic Wind Tunnel for use with heavy gas, allowed for tiltrotor whirl flutter investigations at more representative Reynolds Numbers [14].

Work has continued to this day, with the focus now shifted to a V-22 model known as the WRATS (Wing and Rotor Aeroelastic Test System) semi-span tiltrotor. Experimental [15, 14, 16] and numerical investigations [17, 18] have been conducted on such a model with close comparison found between the results.

Kreshock in 2017 presented results of the comparison between the developed CAMRAD and RCAS models of the WRATS to experimental data [17]. However, limited success was found in the comparison of the experimental and numerical results, and hence an investigation was conducted by Yeo in 2017 in which a simplified model of the WRATS was studied using the CAMRAD and RCAS methods [18]. The complexity of this simplified model was gradually increased within the investigation with an excellent agreement between both analytical models found.

In addition to this work, Hoover in 2017 conducted a numerical investigation into the stiff-inplane WRATS model looking into the predicted loads and whirl flutter stability [19]. This model was studied experimentally by Nixon [15] with a comparison between the RCAS, CAMRAD and Dymore numerical methods conducted. Results of this investigation found a close agreement for the steady hub forces and moments, however some of the higher harmonics within the vibratory blade loads were not captured. In addition to this, the trends of the chordwise and torsional modes of the model are captured, however an under-prediction of the damping and over-prediction of the frequencies were found for the chordwise mode.

Along with investigations into the comparison between experimental and numerical methods, Floros in 2017 conducted an exploratory numerical investigation using RCAS to study the effect of using active wing tips to augment the motion of the tiltrotor nacelle [20]. A scaled XV-15 aircraft was

used for the investigation with a simple PID controller used for the wing tip. The effect of the controller feedback, size and response of the tip was investigated to determine the most effective configuration for suppressing whirl flutter. This investigation found the wing tips to be effective in increasing the stability boundary of this model.

In addition to the work conducted at NASA, interest in a European tiltrotor design along with the enhancement of commercial tools such as NASTRAN has allowed for further investigations to be conducted. Work has been conducted on turbo-prop aircraft [21] and tiltrotors, which was part of the ADYN project looking into the development of the ERICA aircraft [22, 23].

The presented literature survey highlights the lack of numerical work using high-fidelity computational fluid dynamics (CFD). CFD is a low-cost alternative to experimental investigations and has the ability to capture the non-linear aerodynamics present within such engineering applications. As a result, the aim of this investigation is to conduct numerical whirl and stall flutter investigation using the HMB3 CFD solver of the University of Glasgow, coupled with NASTRAN structural models.

## 2 COUPLED METHODOLOGY

### 2.1 HMB3 CFD Solver

The Helicopter Multi-Block (HMB) [24, 25, 26] code is used as the CFD solver for the present work. It solves the Unsteady Reynolds Averaged Navier-Stokes (URANS) equations in integral form using the Arbitrary Lagrangian Eulerian (ALE) formulation for time-dependent domains. The Navier-Stokes equations are discretised using a cell-centered finite volume approach on a multi-block grid,

$$(1) \quad \frac{d}{dt}(\mathbf{W}_{i,j,k} V_{i,j,k}) = -\mathbf{R}_{i,j,k}(\mathbf{W})$$

where  $i, j, k$  represent the cell index,  $\mathbf{W}$  and  $\mathbf{R}$  are the vector of conservative flow variables and flux residual respectively, and  $V_{i,j,k}$  is the volume of the cell  $i, j, k$ .

HMB3 CFD solver has been used in the past to model the flow around a number of engineering applications. This includes the flow around tiltrotor aircraft which was validation by Jimenez *et al.* in 2017 [27].

## 2.2 NASTRAN Structural Model

The structural modelling of the test case can be derived via a stick or plate finite element model. Stick models have the advantage of being simpler to solve with the modes and frequencies captured to an acceptable standard, however, due to the two-dimensional limitations, mesh density can have a significant effect on the overall result. As a result, there must be careful consideration of the amount of elements used within the two-dimensional system.

In addition to simple stick models, more comprehensive plate models can also be used. Such models allow for the chordwise distribution of the structural properties and capture more accurately the modes and frequencies of the test case. Such models increase the modelling complexity and therefore become harder to solve.

From the literature, a combination of stick and plate models have been used. In 1999, Acree developed a stick model for the analysis of the XV-15 [11]. Such a model included structural elements for the wing with rigid bars and concentrated masses used for the nacelle and rotor, respectively. Following this, Acree conducted studies into the V-22 aircraft using a NASTRAN developed plate model and this was utilised within CAMRAD [10]. The use of non-linear stick models has continued to this day, with such models used within the work of Yeo [18] and Hoover [19] looking into whirl flutter within the WRATS tiltrotor model via the RCAS and CAMRAD simulation tools.

## 2.3 Coupling Procedure

To couple the CFD and CSD computations, the following procedure is conducted. The method involves the initial deformation of the blade surface using the Constant Volume Tetrahedron (CVT) [28] method, with the block vertex positions updated via the spring analogy method (SAM) [29], before the full mesh generation via a Transfinite Interpolation (TFI) [30]. This procedure is extensively described by Dehaeze in 2012 [31]. The TFI firstly interpolates the block edges and faces from the new vertex position, and then interpolates the full mesh from the outer surfaces of each block. This method uses the properties of multi-block meshes and maintains its efficiency as the number of blocks increases, particularly in the span-wise blade direction.

For forward flying rotors, a modal approach is used. The modal approach allows a reduction of the problem size by modelling the blade shape as the sum of a limited number of dominant eigenmodes, which are obtained via the NASTRAN model. The blade shape is described as follows:

$$(2) \quad \psi = \psi_0 + \sum_{i=1}^{n_m} \alpha_i \psi_i,$$

where  $\psi$  is the blade shape,  $\psi_0$  the blade static deformation, and  $\psi_i$  is the  $i$ -th mass-scaled eigenmode of the blade. The amplitude coefficients,  $\alpha_i$ , are obtained by solving the equations:

$$(3) \quad \frac{\partial^2 a_i}{\partial t^2} + 2\xi_i \omega_i \frac{\partial a_i}{\partial t} + \omega_i^2 a_i = f_i \psi_i,$$

where  $\omega_i$  and  $\xi_i$  are the eigenfrequencies and the eigenmode damping ratios, respectively,  $f_i$  are the vector of external force components. To solve Equation 3 in time, along with the flow solution around the rotor, a strong coupling method is used.

The strong coupling approach does not force periodicity in the blade deformation and may need more time to solve a problem. It may also be less stable than weakly-coupled methods, however, it allows more flexibility for complex motions of the helicopter which are not linked to a steady flight condition.

Since HMB3 performs time-marching computations using the dual-time step method, one could opt to exchange information between the structural model and the aerodynamic model either at the end of each real-time step or at the end of each Newton sub-iteration. Of course, exchanging information at each Newton step results in more consistent solutions. On the other hand, if the real time-step is small, fewer exchanges between the CFD and CSD methods would result. As a result, two approaches were tested and compared: a leap-frog method (method 1) which computes the modal amplitudes between each real time step, and a strongly implicit method (method 2) which computes the modal amplitudes between each pseudo-time step.

## 3 CFD COMPUTATIONS

To highlight the non-linear features present within such tiltrotor test cases, a steady simulation of

the XV-15 propeller blade was conducted. For this computation, the equations of motion were cast within a non-inertial reference frame, thus allowing for a steady computation.

An chimera mesh was derived containing 7 million cells, with the domain shown in Figure 1. The geometry was scaled as per the blade chord with a Reynolds number of 16.6 million and tip Mach number of 0.69. The standard  $k - \omega$  turbulence model [32] was used for this simulation.

Due to the lack of experimental data, a comparison to the numerical simulation of Kaul [33] in terms of surface pressure coefficient is shown in Figure 2. As can be seen, a close matched between the pressure coefficients is found at the 0.72 and 0.94 radial positions.

Such validation allows for the evaluation of the non-linear flow features present within the tiltrotor blade. This can be seen via the extraction of the iso-surfaces based upon a Q-Criteria of 0.01. This is shown in Figure 4. As can be seen from the visualisation, the blade tip vortex is within range of interacting with the following blade. The peak blade loading was found at the blade tip and depending on the required thrust, the interacting tip trailing vortex could induce stall flutter. In addition to this, a high amount of non-linear aerodynamics are captured towards the blade root. Such flow structures may couple with the nacelle structural model and thus induce whirl flutter.

## 4 SIMPLE WHIRL FLUTTER MODEL

A simple whirl flutter model was initially derived based on the analytical method of Reed [3], with two degrees of freedom in pitch and yaw. This simple model involves the quasi-steady calculation of the forces and moments on the propeller with aerodynamic derivatives used to capture the

force and moment responses to a change in position and rate. Such aerodynamic derivatives can be calculated analytically [2] with an approximation published by de Young in 1965 [34]. This is used with a rotational spring-damper system modelled with rigid beams to capture the structure. The schematic of this system can be seen in Figure 5. Based upon this schematic, the equations of motion of the system were derived via Lagrange's equation, with the force term resulting from the decoupled aerodynamics (Equation 4).

For this equation of motion,  $\mathbf{D}$  and  $\mathbf{K}$  represents the structural damping and stiffness matrices, respectively, with  $\mathbf{D}^A$  and  $\mathbf{K}^A$  representing the aerodynamic damping and stiffness, respectively. Matrix  $\mathbf{G}$  contains the gyroscopic terms with the structural mass found within  $\mathbf{M}$ .

The structural and gyroscopic matrices can be seen in Equation 5. These contain the mass moment of inertia's within the X ( $J_x$ ), Y ( $J_y$ ) and Z ( $J_z$ ) directions for the structural model. In addition to this, the stiffness ( $K$ ) and damping ( $\gamma$ ), within pitch ( $\theta$ ) and yaw ( $\psi$ ), of the rotational spring damper component can be found within the damping and stiffness matrices. The gyroscopic matrix additionally contains the propeller rotational velocity ( $\Omega$ ).

The aerodynamic terms can be seen in Equation 6 and these are determined via the aerodynamic derivatives  $c_{n\theta}$ ,  $c_{z\theta}$ ,  $c_{yq}$ , and  $c_{mq}$ . These represent the side and vertical force,  $y$  and  $z$ , respectively, and pitch and yaw moment,  $m$  and  $n$ , respectively, with respect to the pitch angle,  $\theta$  and pitch rate,  $q$ . In addition to this, the distance between the propeller disc and engine attachment point ( $a$ ) is taken into account, along with the propeller diameter ( $D_p$ ).

The combination of the structural and aerodynamic forcing components within the derived equation of motion allows for an eigenvalue analysis to be conducted in order to determine the stability boundary of the system. To highlight the use of this model, two test cases have been conducted.

$$(4) \quad \left( -\omega^2 [\mathbf{M}] + j\omega \left( [\mathbf{D}] + [\mathbf{G}] + q_\infty F_p \frac{D_p^2}{V_\infty} [\mathbf{D}^A] \right) + ([\mathbf{K}] + q_\infty F_p D_p [\mathbf{K}^A]) \right) \begin{bmatrix} \bar{\Theta} \\ \bar{\Psi} \end{bmatrix} = \{0\}$$

$$(5) \quad \begin{aligned} [\mathbf{M}] &= \begin{bmatrix} J_y & 0 \\ 0 & J_z \end{bmatrix} \\ [\mathbf{D}] &= \begin{bmatrix} \frac{K_\theta \gamma_\theta}{\omega} & 0 \\ 0 & \frac{K_\psi \gamma_\psi}{\omega} \end{bmatrix} \\ [\mathbf{K}] &= \begin{bmatrix} K_\theta & 0 \\ 0 & K_\psi \end{bmatrix} \\ [\mathbf{G}] &= \begin{bmatrix} 0 & J_x \Omega \\ -J_x \Omega & 0 \end{bmatrix} \end{aligned}$$

$$(6) \quad \begin{aligned} [\mathbf{K}^A] &= \begin{bmatrix} \frac{ac_{z\theta}}{D_p} & c_{n\theta} + \frac{ac_{y\theta}}{D_p} \\ -c_{n\theta} - \frac{ac_{y\theta}}{D_p} & \frac{ac_{z\theta}}{D_p} \end{bmatrix} \\ [\mathbf{D}^A] &= \begin{bmatrix} -\frac{c_{mq}}{2} - \frac{a^2 c_{z\theta}}{D_p^2} & \frac{ac_{yq}}{2D_p} - \frac{ac_{n\theta}}{D_p} - \frac{a^2 c_{y\theta}}{D_p^2} \\ -\frac{ac_{yq}}{2D_p} + \frac{ac_{n\theta}}{D_p} + \frac{a^2 c_{y\theta}}{D_p^2} & -\frac{c_{mq}}{2} - \frac{a^2 c_{z\theta}}{D_p^2} \end{bmatrix} \end{aligned}$$

#### 4.1 Standard Propeller Test Case

An initial investigation was conducted on the standard propeller used by Reed in 1961 [3]. This is a four bladed propeller of constant chord outboard of  $0.3x/r$ , and a linear twist (Figure 6). The structural properties for this investigation can be seen in Table 1. These parameters were taken from the analysis conducted by Reed, with the stiffnesses selected to correlate with experimental data of a simple demonstrator system.

Before conducting the stability analysis, a comparison of the derived aerodynamic derivatives obtained from Ribner's method [2], an approximation of Ribner's method [34], and results of Reed was conducted. As can be seen in Figure 7, a large amount of scatter was found within the results, however the trends of the derivatives, with respect to the pitching angle of the propeller, were met.

Following this, a stability analysis was conducted using the approximation of Ribner's method. Figure 8 shows the stability boundary obtained for this standard propeller in terms of the propeller rotational velocity, with a comparison made to the results of Reed and some experimental results. As shown, a closer match to the experimental results was found with the difference between the numerical techniques related to the scatter within the aerodynamic derivatives.

#### 4.2 XV-15 Tiltrotor Test Case

In addition to the standard propeller test case, the XV-15 tiltrotor blade was investigated in terms of its whirl flutter boundary. For this analysis the number of blades, propeller radius, inertia's and the attachment distance were selected to match the data found within the technical report of Maisel [35]. These parameters can be seen within Table 2.

A comparison of the XV-15 blade to the standard propeller is shown in Figure 9, and as can be seen, a decrease in the stability boundary was found for the XV-15 blade. This reduction in the whirl flutter boundary was found due to the increase of the inertias, specifically the mass moment of inertia in the x-direction ( $J_x$ ). Figure 9 highlights the change in the whirl flutter boundary for the XV-15 blade due to the change in  $J_x$ . Differences of less than one percent are found for the whirl flutter boundary due to a change in the y- and z-direction inertias.

A reduction within the whirl flutter boundary for a tiltrotor blade in comparison to a standard propeller highlights the forward flight limitation of such aircraft. However, the current analysis is outside the operating limits of the XV-15, in terms of the blade rotational velocity. As a result, an analysis of the XV-15 tiltrotor blade within the design operating limits of the blade can be seen in Figure 10. As shown, at the current values of stiffness the flutter velocity is well below the design operating speed of  $170 \text{ knots}$ . To achieve higher velocities, an increase in the rotational stiffnesses by a factor of approxi-

mately four is required. This increase can also be seen in Figure 10.

## 5 CONCLUSION

This paper presents the results of a whirl flutter analysis using a simple two degree of freedom method. As highlighted, a fair amount of scatter can be found within the results. This can be down to the simplification of the aerodynamics and structural model, however close results to experimental data can be found for a standard propeller. This method was also used to study the XV-15 tiltrotor blade, and as shown, a stability boundary can be derived. This boundary can be used to define the range of unsteady CFD computations that are to be conducted. A steady CFD simulation has also been conducted using the XV-15 blade to highlight the ability of the high-fidelity method in deriving accurate solutions.

Future work will consist of the investigation of a coupled CFD-CSD solution.

## 6 ACKNOWLEDGMENTS

The use of the cluster HPC and MIFY of the University of Glasgow is gratefully acknowledged. Some results were obtained using the EPSRC funded ARCHIE-WeSt High Performance Computer ([www.archie-west.ac.uk](http://www.archie-west.ac.uk)), EPSRC grant no. EP/K000586/1.

## 7 REFERENCES

- [1] Reed, W., "Review of Propeller-Rotor Whirl Flutter," Tech. Rep. R-264, National Aeronautics and Space Administration, 1967.
- [2] Ribner, H., "Propellers in Yaw," Tech. Rep. 820, National Advisory Committee for Aeronautics, 1945.
- [3] Reed, W. and Bland, S., "An Analytical Treatment of Aircraft Propeller Precession Instability," Tech. Rep. D-659, National Aeronautics and Space Administration, 1961.
- [4] Abbott, F., Kelly, H., and Hampton, K., "Investigation of Propeller-Power-Plant Autoprecession Boundaries for a Dynamic-Aeroelastic Model of a Four-Engine Turboprop Transport Airplane," Tech. Rep. D-1806, National Aeronautics and Space Administration, 1963.
- [5] Bennett, R. and Bland, S., "Experimental and Analytical Investigation of Propeller Whirl Flutter of a Power Plant on a Flexible Wing," Tech. Rep. D-2399, National Aeronautics and Space Administration, 1964.
- [6] Bland, S. and Bennett, R., "Wind-Tunnel Measurement of Propeller Whirl-Flutter Speeds and Static-Stability Derivatives and Comparison with Theory," Tech. Rep. D-1807, National Aeronautics and Space Administration, 1963.
- [7] Johnson, W., "A Comprehensive Analytical Model of Rotorcraft Aerodynamics and Dynamics: Part I: Analysis Development," Technical Memorandum 81182, National Aeronautics and Space Administration, 1980.
- [8] Leishman, J. and Beddos, T., "A Semi-Empirical Model for Dynamic Stall," *Journal of the American Helicopter Society*, Vol. 34, No. 3, 1989.
- [9] Jr, C. A., "An Improved CAMRAD Model for Aeroelastic Stability Analysis of the XV-15 with Advanced Technology Blades," Technical Memorandum 4448, National Aeronautics and Space Administration, 1993.
- [10] Jr, C. A., "Effects of V-22 blade modifications on whirl flutter and loads," *Journal of the American Helicopter Society*, Vol. 50, No. 2, 2005.
- [11] Jr, C. A., Peyran, R., and Johnson, W., "Rotor Design for Whirl Flutter: An Examination of Options for Improving Tiltrotor Aeroelastic Stability Margins," *55th Annual Forum*, American Helicopter Society, 1999.
- [12] Jr, C. A., Peyran, R., and Johnson, W., "Rotor Design Options for Improving Tiltrotor Whirl-Flutter Stability Margins," *Journal of the American Helicopter Society*, Vol. 46, No. 2, 2001.
- [13] Jr, C. A. and Tischler, M., "Determining XV-15 Aeroelastic Modes from Flight Data with Frequency-Domain Methods," Technical Paper 3330, National Aeronautics and Space Administration, 1993.
- [14] Piatak, D., Kvaternik, R., Nixon, M., Langston, C., Singleton, J., Bennett, R., and Brown,

- R., "A Parametric Investigation of Whirl-Flutter Stability on the WRATS Tiltrotor Model," *Journal of the American Helicopter Society*, Vol. 47, No. 2, 2002.
- [15] Nixon, M., Langston, C., Singleton, J., Piatak, D., Kvaternik, R., Corso, L., and Brown, R., "Aeroelastic Stability of a Four-Bladed Semi-Articulated Soft-Inplane Tiltrotor Model," *59th Annual Forum*, The American Helicopter Society, 2003.
- [16] Newman, J., Parham, T., Johnson, C., and Popelka, D., "Wind Tunnel Test Results for a 0.2 Scale 4-Bladed Tiltrotor Aeroelastic Model," *70th Annual Forum*, American Helicopter Society, 2014.
- [17] Kreshock, A. and Yeo, H., "Tiltrotor Whirl-Flutter Stability Predictions Using Comprehensive Analysis," *AIAA SciTech Forum*, 2017.
- [18] Yeo, H., Bosworth, J., Jr, C. A., and Kreshock, A., *73rd Annual Forum*, American Helicopter Society.
- [19] Hoover, C., Shen, J., Kang, H., and Kreshock, A., *73rd Annual Forum*, American Helicopter Society.
- [20] Floros, M. and Kang, H., *73rd Annual Forum*, American Helicopter Society.
- [21] Cecrdle, J., *Whirl Flutter of Turboprop Aircraft Structures*, Woodhead Publishing, 1st ed., 2015.
- [22] Gennaretti, M., *Risposta e Stabilita Aeroelastica di Velivoli Tiltrotor*, Ph.D. thesis, Universita degli Studi Roma Tre, 2008.
- [23] Maffei, F., *Analisi di Whirl Flutter per un Convertiplano di Nuova Generazione*, Ph.D. thesis, Universita Degli Studi di Napoli FED-ERICO II, 2007.
- [24] Lawson, S. J., Steijl, R., Woodgate, M., and Barakos, G. N., "High performance computing for challenging problems in computational fluid dynamics," *Progress in Aerospace Sciences*, Vol. 52, No. 1, 2012, pp. 19–29, DOI: 10.1016/j.paerosci.2012.03.004.
- [25] Steijl, R. and Barakos, G. N., "Sliding mesh algorithm for CFD analysis of helicopter rotor-fuselage aerodynamics," *International Journal for Numerical Methods in Fluids*, Vol. 58, No. 5, 2008, pp. 527–549, DOI: 10.1002/d.1757.
- [26] Steijl, R., Barakos, G. N., and Badcock, K., "A framework for CFD analysis of helicopter rotors in hover and forward flight," *International Journal for Numerical Methods in Fluids*, Vol. 51, No. 8, 2006, pp. 819–847, DOI: 10.1002/d.1086.
- [27] Jimenez-Garcia, A., Barakos, G., and Gates, S., "Tiltrotor CFD Part I - Validation," *The Aeronautical Journal*, Vol. 121, No. 1239, 2017.
- [28] Goura, G., Badcock, K., Woodgate, M., and Richards, B., "Implicit Method for the Time Marching Analysis of Flutter," *The Aeronautical Journal*, Vol. 105, No. 1046, 2001.
- [29] Blom, F., "Considerations on the Spring Analogy," *International Journal for Numerical Methods in Fluids*, Vol. 32, No. 6, 2000.
- [30] Dubuc, L., Cantariti, F., Woodgate, M., Gribben, B., Badcock, K., and Richards, B., "A Grid Deformation Technique for Unsteady Flow Computations," *International Journal for Numerical Methods in Fluids*, Vol. 32, No. 3, 2000.
- [31] Dehaeze, F. and Barakos, G., "Mesh Deformation Method for Rotor Flows," *Journal of Aircraft*, Vol. 49, No. 1, 2012.
- [32] Wilcox, D., "Multiscale model for turbulent flows," *AIAA Journal*, 1988.
- [33] Kaul, U., "Effect of Inflow Boundary Conditions on Hovering Tilt-Rotor Flows," *7th International Conference on Computational Fluid Dynamics*, 2012.
- [34] Young, J. D., "Propeller at High Incidence," *Journal of Aircraft*, Vol. 2, No. 3, 1965.
- [35] Maisel, M., "Tilt rotor research aircraft familiarization document," Technical Memorandum X-62, 407, National Aeronautics and Space Administration, 1975.

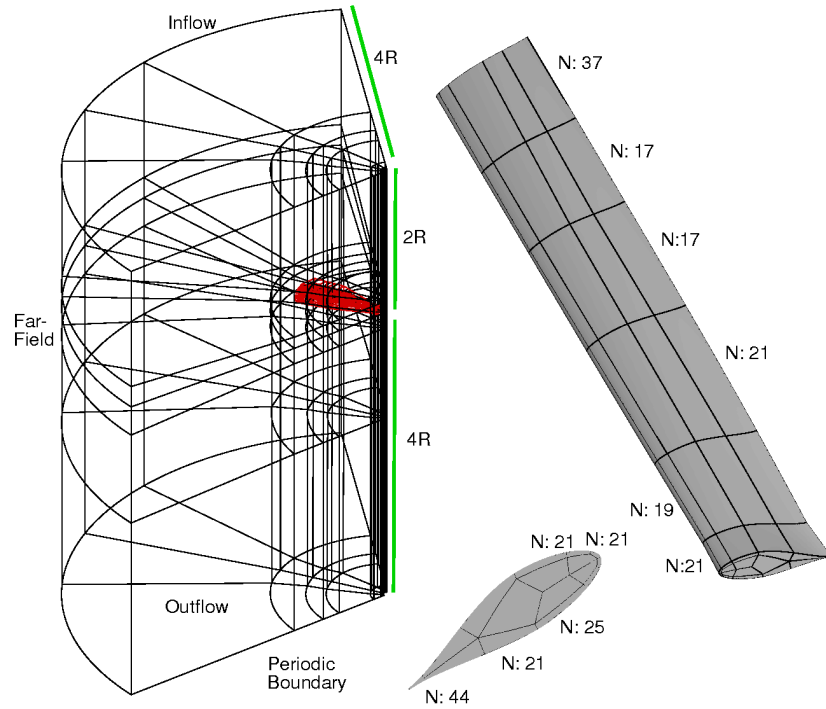
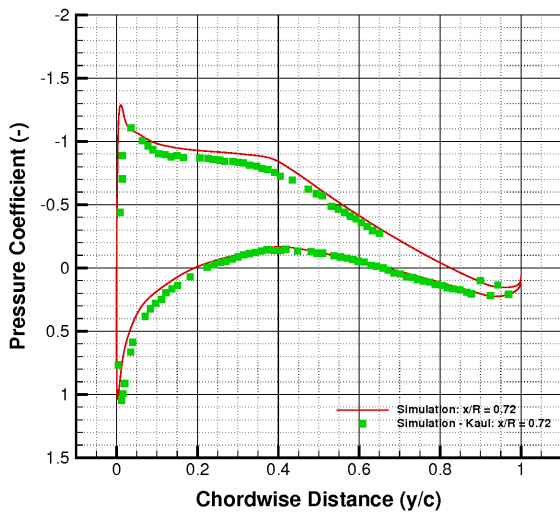
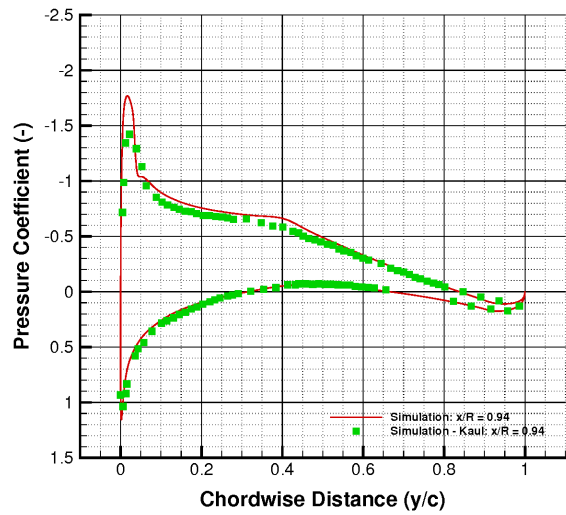


Figure 1: Steady CFD Simulation, XV-15 Tiltrotor Blade: Chimera Grid



(a)



(b)

Figure 2: Steady CFD Simulation, XV-15 Tiltrotor Blade: Surface Pressure Coefficient

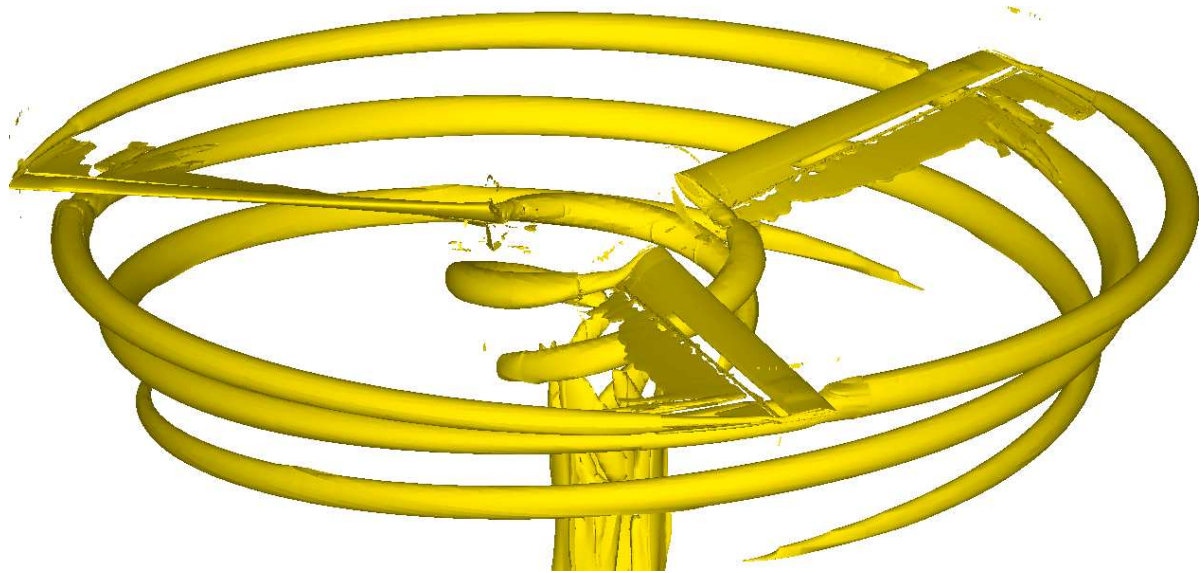


Figure 3: Steady CFD Simulation, XV-15 Tiltrotor Blade: Wake Visualisation (Iso-surfaces of Q-Criteria 0.01)

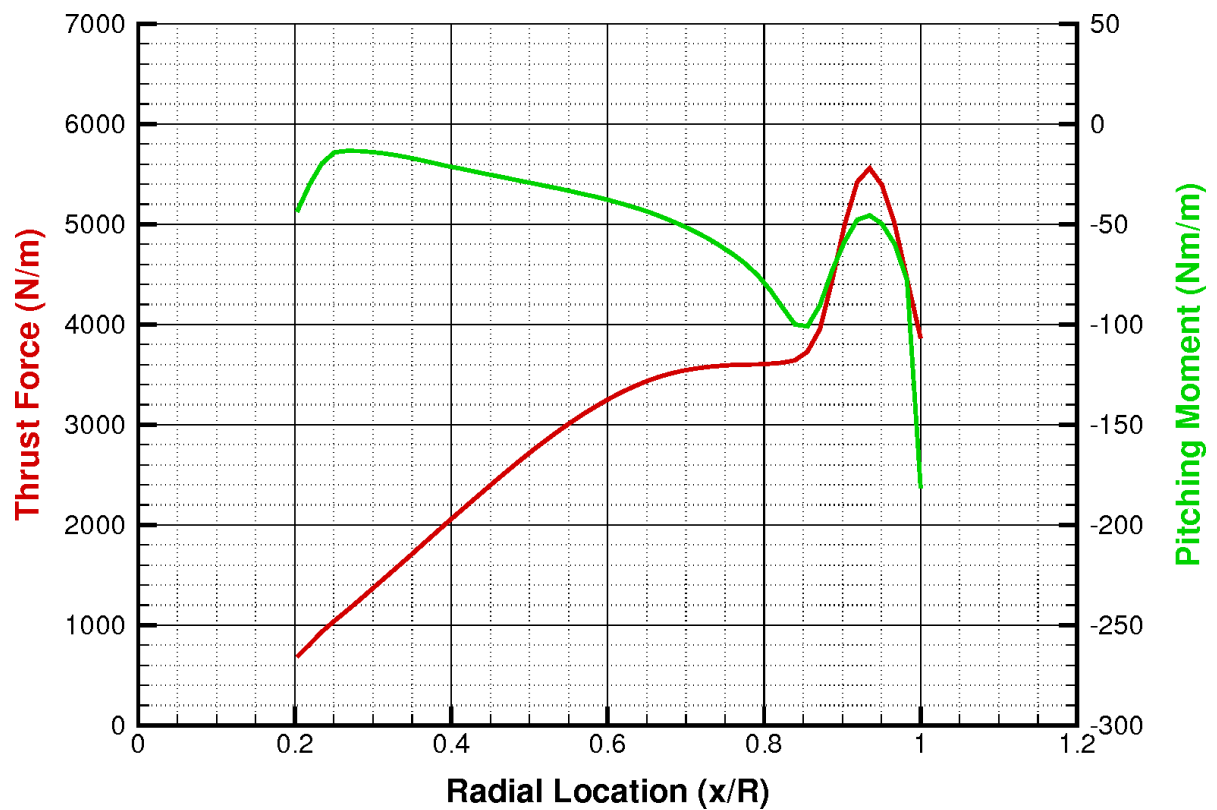


Figure 4: Steady CFD Simulation, XV-15 Tiltrotor Blade: Extracted Loads

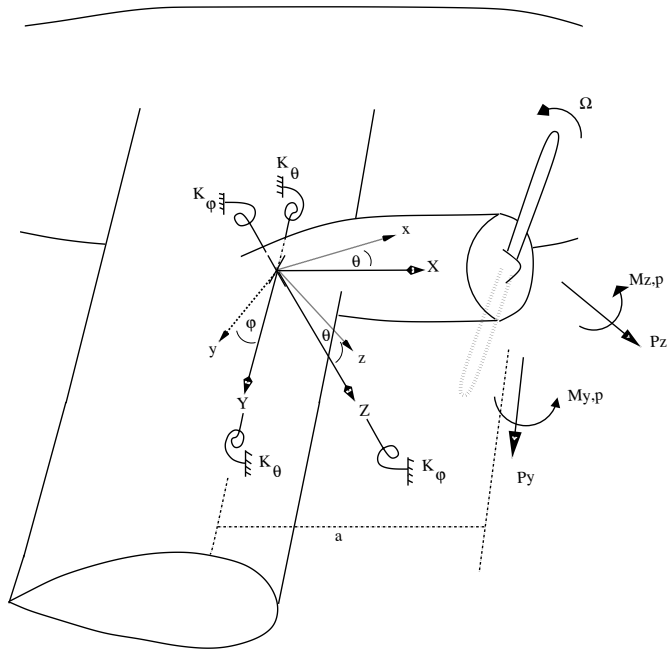


Figure 5: Simple Whirl Model Schematic

Table 1: Simple Whirl Model: Standard Propeller Test Case

Number of Blades (-)	4
Lift Curve Slope (/rad)	6.28
Propeller Radius (m)	2.05
Reference Structural Damping (-)	0.014
Reference Structural Stiffness ( $Nm/rad$ )	$0.91 \times 10^6$
Mass Moment of Inertia ( $kgm^2$ ) [x,y,z]	238, 1870, 1870
Attachment Distance (m)	0.0648

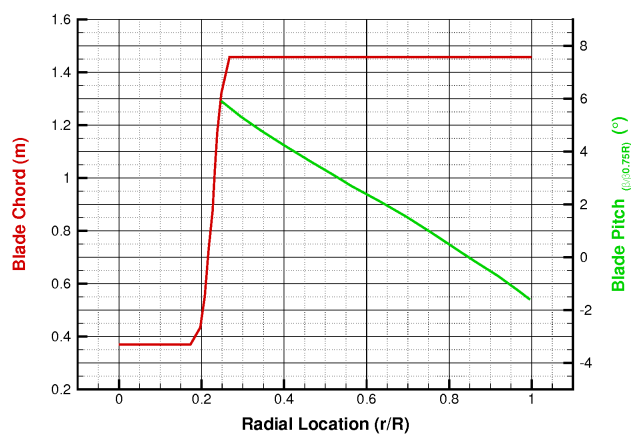
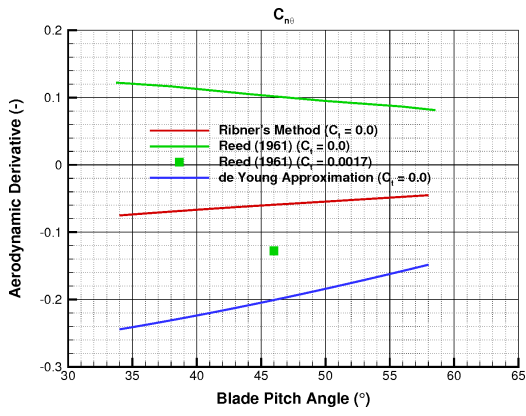
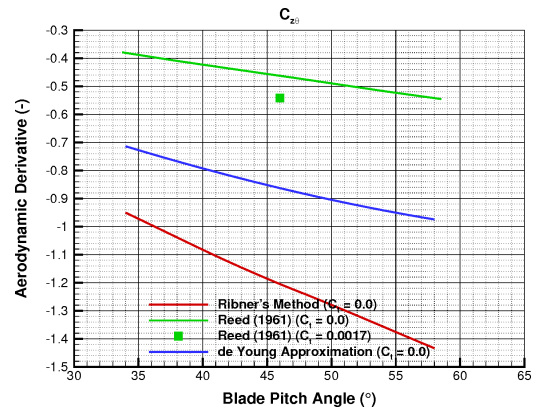


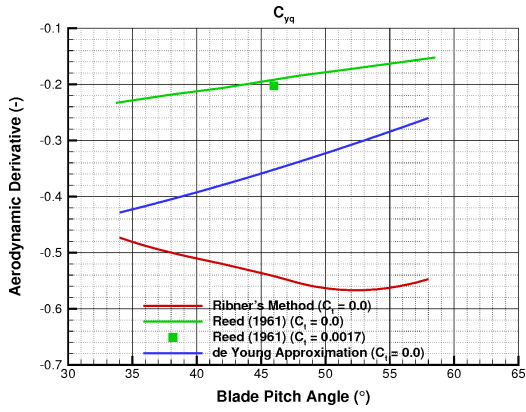
Figure 6: Simple Whirl Model: Standard Propeller Blade Properties



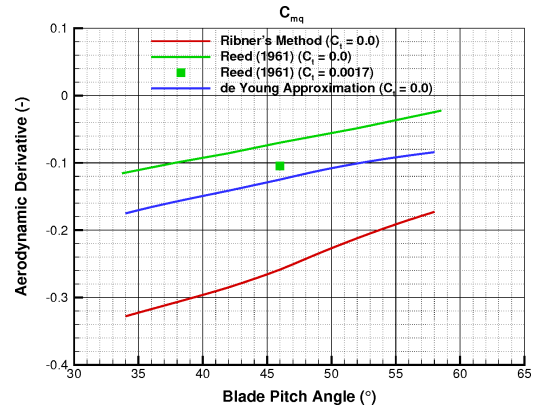
(a) Yawing moment due to pitch angle



(b) Vertical force due to pitch angle



(c) Side force due to pitch rate



(d) Pitching moment due to pitch rate

Figure 7: Simple Whirl Model: Standard Propeller Aerodynamic Derivatives

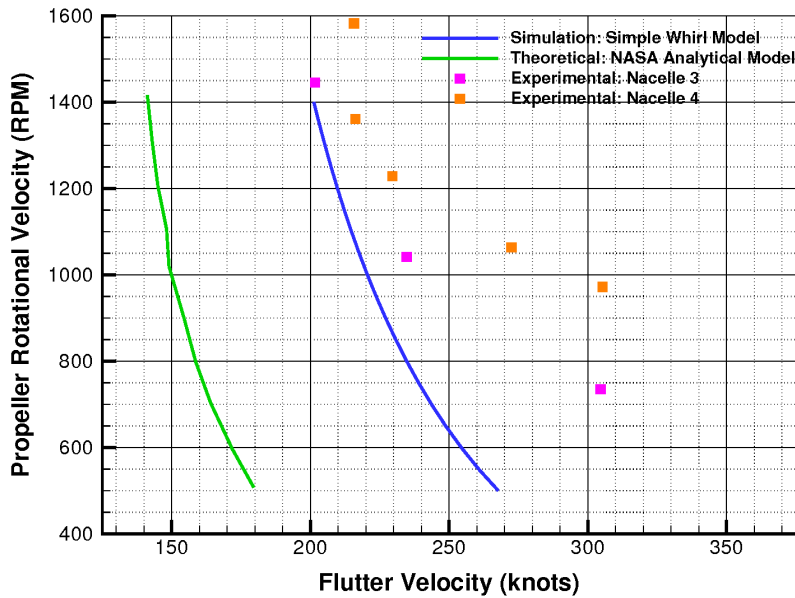


Figure 8: Simple Whirl Model: Standard Propeller Whirl Flutter Stability Boundary

Table 2: Simple Whirl Model: XV-15 Test Case

Number of Blades (-)	3
Propeller Radius (m)	3.81
Reference Structural Damping (-)	0.014
Reference Structural Stiffness ( $Nm/rad$ )	$0.91 \times 10^6$
Mass Moment of Inertia ( $kgm^2$ ) [x,y,z]	54910, 17896, 68197
Attachment Distance (m)	2.413

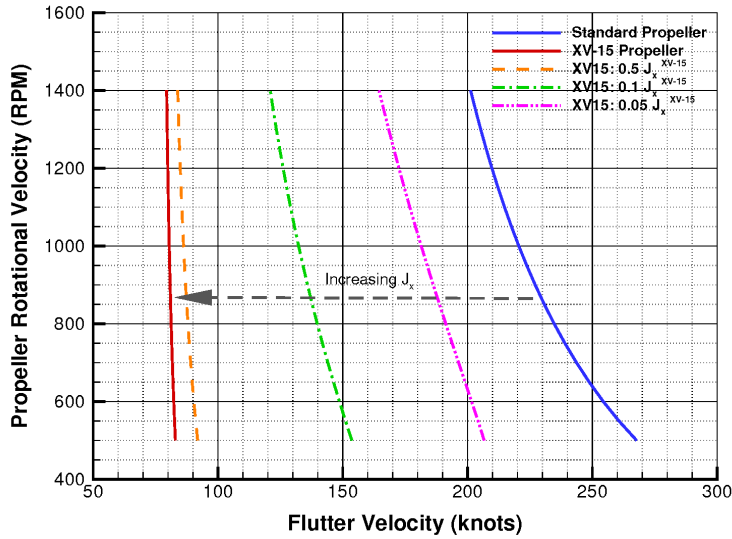


Figure 9: Simple Whirl Model: XV-15 Whirl Flutter Stability Boundary

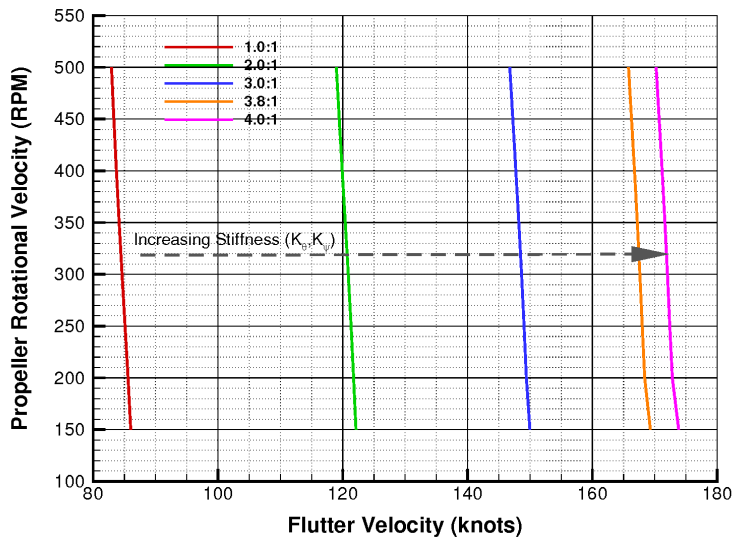


Figure 10: Simple Whirl Model: XV-15 Whirl Flutter Stability Boundary with Stiffness Variation